

## Experimental study of flight effects on screech in underexpanded jets

Benoît André,<sup>1,a)</sup> Thomas Castelain,<sup>1,2,b)</sup> and Christophe Bailly<sup>1,3,c)</sup>

<sup>1</sup>Laboratoire de Mécanique des Fluides et d'Acoustique, UMR CNRS 5509, Ecole Centrale de Lyon, Université de Lyon, 36 Avenue Guy de Collongue, 69134 Ecully Cedex, France

<sup>2</sup>Université Lyon 1, 43 Boulevard du 11 Novembre 1918, 69622 Villeurbanne Cedex, France

<sup>3</sup>Institut Universitaire de France, Paris, France

(Received 9 June 2011; accepted 23 November 2011; published online 30 December 2011)

Flight effects on screech from an underexpanded supersonic jet have been experimentally investigated in a free jet facility. Screech frequency prediction is addressed, and some conclusions about the convection velocity under flight conditions are drawn. An azimuthal near field acoustic antenna is used to investigate the modal behaviour of screech with forward flight effects. Several mode switchings are identified as the flight velocity is increased but none can be related to a change in the screech azimuthal mode content. Screech is enhanced by flight at high fully expanded Mach number  $M_j$ . This conclusion, established from acoustic far field measurements, is supported by the analysis of schlieren visualizations. © 2011 American Institute of Physics. [doi:10.1063/1.3671735]

### I. INTRODUCTION

Underexpanded supersonic jets usually emit two so-called shock associated noise components beside the mixing noise also present in subsonic jets: the broadband shock associated noise and a tonal noise referred to as screech. Screech has been extensively studied since Powell's pioneering work.<sup>1</sup> Powell explained with some success the generation of this tone by an acoustic feedback loop. In this model, vorticity disturbances originating from the nozzle lip are convected downstream and interact with the shock cell pattern of the jet plume. The acoustic waves emanating from this interaction propagate back to the nozzle where they trigger new disturbances, thus closing the loop. This loop is resonant for some frequencies which are the fundamental screech frequency and its harmonics. For circular jets, Powell<sup>1</sup> isolated four modes, A, B, C, and D, from the screech frequency evolution with increasing nozzle pressure ratio (NPR), defined as the ratio of the upstream stagnation pressure to the ambient pressure. Each mode switching was characterized by a frequency jump, and each mode was dominant over a rather well defined NPR range. Later, Merle<sup>2</sup> pointed out that mode A could be divided into modes A1 and A2. Davies and Oldfield<sup>3,4</sup> subsequently studied the acoustic emission using two microphones located on either side of the jet and associated the modes with emission patterns. A1 and A2 were, thus, classified as being axisymmetric, B sinuous, and C helical. Mode D longer resisted classification, but is now known to be sinuous. More recently, Tam *et al.*<sup>5</sup> proposed a more elaborate model for screech generation based on a description of the relevant turbulent structures as instability waves. The modal characteristics of screech were

studied in detail by Powell *et al.*<sup>6</sup> with measurements of frequency and convection velocity, estimation of source location, and focus on the screech unstable behaviour. Screech modes were investigated in light of the jet instability theory by Powell *et al.*<sup>6</sup> and Ponton and Seiner,<sup>7</sup> accrediting the instability wave description mentioned above. A summary of the knowledge on screech is provided in Raman.<sup>8,9</sup>

Hay and Rose<sup>10</sup> reported that screech could arise on an aircraft in flight and could lead to structural damage. However, as pointed out by Tam,<sup>11</sup> screech in flight has not yet been studied in sufficient detail.

Modifications of jet noise in flight are of interest in aeronautics. The end of the 1970s, thus, saw considerable effort, both experimental and theoretical, devoted to understanding the noise source modifications due to forward motion. An extensive review on this topic was provided in the introduction of Michalke and Michel.<sup>12</sup> Among the early works, Hay and Rose<sup>10</sup> and Bryce and Pinker<sup>13</sup> addressed the problem of noise from shock containing jets in forward motion. They proposed an extension of the screech frequency prediction formula to the flight case. This particular problem was further looked at by Norum and Shearin<sup>14</sup> and by Krothapalli *et al.*<sup>15</sup> Norum and Shearin<sup>16</sup> also showed that the screech amplitude is barely modified when the flight Mach number is increased up to 0.4. This conclusion is in agreement with the data of Krothapalli *et al.*<sup>15</sup> but somewhat different from a recent publication by Viswanathan and Czech.<sup>17</sup> The study of Brown *et al.*,<sup>18</sup> where flight Mach numbers go up to 0.8, also suggests a reduction of screech at high flight velocities but the screech contribution to the overall sound pressure levels (OASPLs) was very weak in their work, even under static conditions. Finally, the occurrence of mode switching in flight was reported by Norum and Shearin<sup>14</sup> and Norum and Brown.<sup>19</sup> In the former reference, the dominant screech mode for a fully expanded jet Mach number  $M_j$  of 1.67 was seen to switch from C to B between static conditions and a

<sup>a)</sup>Electronic mail: benoit.andre@ec-lyon.fr.

<sup>b)</sup>Electronic mail: thomas.castelain@ec-lyon.fr.

<sup>c)</sup>Electronic mail: christophe.bailly@ec-lyon.fr.

flight Mach number  $M_f$  of 0.15. In addition, mode C was not found to dominate at any jet operating conditions in flight. This was later confirmed by Norum and Shearin,<sup>16</sup> in whose work the appearance of new modes at  $M_j > 1.55$  was identified.

To summarize, few studies have been devoted to the study of screech from jets in forward motion. Moreover, the existing ones usually concentrate on screech frequency prediction. No consensus has been reached on the effect of flight on screech strength, and the modal behaviour of screech in flight seems only to have been studied through the analysis of the screech frequency evolution. The present study has been undertaken as a step toward a better understanding of the phenomenon of screech in flight. It is part of a larger study of flight effects on shock associated noise, which is going to be responsible for a dominant part of cabin noise levels in cruise condition for the next-generation commercial aircraft including composite fuselage. In this perspective, the noise from cold circular supersonic jets is relevant. This configuration is tested herein.

This paper is organized as follows. First, the experimental facility is presented in Sec. II. Then, the screech frequency prediction for static and forward flight conditions is addressed in Sec. III. Flight effects on the screech modal behaviour are investigated in Sec. IV. Finally, effects of forward motion on screech amplitude are identified from acoustic measurements as well as analysis of schlieren flow visualizations in Sec. V.

## II. EXPERIMENTAL SET-UP

### A. The facility

Flight is simulated in the present experiment by means of a free jet facility, where the underexpanded supersonic jet is embedded in a larger free flow. In the following, the supersonic jet will also be called primary or model jet while the free jet will also be referred to as secondary or subsonic jet. The two jets exhaust in the  $10 \times 8 \times 8$  m<sup>3</sup> large anechoic room of the Centre Acoustique. The supersonic flow originates from a continuously operating compressor fed with dry air while the subsonic one is generated by a fan system. Both jets are unheated. Within the anechoic room, well upstream of the jet exit, the supersonic duct penetrates into the subsonic flow. In the final section before the exit, both ducts are cylindrical and coaxial. The supersonic duct is maintained at its central position inside the secondary tunnel by a set of 12% thick zero lift airfoil sections. The primary jet exhausts through a  $D = 38$  mm diameter axisymmetric contoured convergent nozzle of 0.5 mm lip thickness. The secondary duct is terminated by a 200 mm diameter round contoured convergent nozzle, and both flows have the same exit plane. In the following, the origin of the coordinates is taken at the center of the nozzles. The flow set-up can be seen in Fig. 1.

The primary jet is monitored by measuring the wall static pressure 15 nozzle diameters upstream of the exit. Stagnation pressure is then retrieved from the static pressure value through an estimate of the local Mach number in the measurement cross section. This value is known by the use of the area Mach number relation (see, e.g., Anderson<sup>20</sup>) with the assumption of a unit exit Mach number. The total temperatures of both flows are measured by thermocouple probes. In this paper, the fully expanded Mach number for the primary

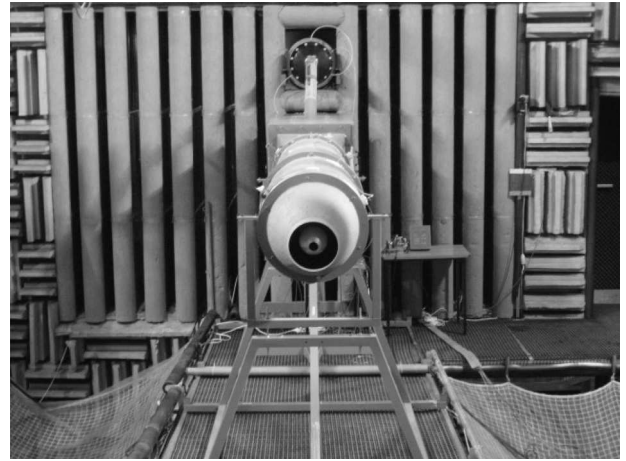


FIG. 1. Photograph of the free jet flight simulating facility built in an anechoic environment.

jet goes up to 1.5 and the flight Mach number up to about 0.4. All experiments reported herein have been conducted with supersonic primary jets whose mean convection velocities are subsonic, so that no strong Mach wave radiation occurs.

The experimental facility has been carefully checked by means of total pressure and hot wire traverses while operating at subsonic conditions to ensure that the flows are axisymmetric. Furthermore, the adequacy of the free jet to model jet diameter ratio to simulate flight conditions for shock associated noise has been verified by measuring the length of the free jet potential core at  $M_j = 0.6$  and  $M_f = 0.28$ . It has been found that the potential core extends up to about  $14 D$ , where  $D$  is the primary nozzle diameter. It has to be noted that the secondary potential core length in coaxial arrangements is known not to depend on the inner to outer velocity ratio (see, e.g., Champagne and Wagnanski<sup>21</sup>).  $14 D$  approximately correspond to 11 shock cells at  $M_j = 1.50$  if we assess the mean shock cell length by the formula from Seiner and Norum,<sup>22</sup>

$$L_s \approx 1.12 (M_j^2 - 1)^{1/2} D.$$

Referring to Davies and Oldfield,<sup>3</sup> screech originates primarily from shock cells located further upstream. The part of the shock-containing jet plume which is relevant for screech generation is embedded in the potential core of the outer flow, and therefore, the free jet to model jet diameter ratio appears sufficient for proper flight simulation.

### B. The measurement techniques

A conventional Z-type schlieren system is used to visualize the flow. It consists of a continuous Quartz Tungsten Halogen light source, two  $f/8$  parabolic mirrors with diameter of 203.2 mm, a razor blade set perpendicular to the flow direction as filter, and a high-speed CMOS camera. This set-up is mounted on a traversing system aligned with the jet axis. Far field acoustic data are obtained from thirteen 6.35 mm diameter PCB Piezotronics condenser microphones fixed on a circular polar antenna 2020 mm or approximately  $53 D$  from the centre of the nozzles. The microphones are located every  $10^\circ$  from  $30^\circ$  to  $150^\circ$ . In the following, polar angles are measured from the downstream jet axis. The

transducers are used in normal incidence without protecting grid as is recommended by Viswanathan.<sup>23</sup> Near field temporal pressure signals are also measured by means of a circular azimuthal antenna laid on the secondary nozzle (see Fig. 2). A similar experimental arrangement has already been used for the study of screech, for example, by Powell *et al.*,<sup>6</sup> Ponton and Seiner,<sup>7</sup> or Massey and Ahuja.<sup>24</sup> Such an arrangement is essential to study screech modes from the phase relations between the microphones. Depending on the case considered, 15 or 18 PCB microphones are located on a 18-hole circular mesh with 20° azimuthal periodicity. All pressure signals are acquired at a rate of 102 400 Hz by a National Instrument PXI 5733 board.

### C. Mach number profiles in the secondary flow

Total and static pressure transverse profiles have been measured across the secondary jet at several values of fan engine speed with no primary jet ( $M_j = 0$ ). Using isentropic relations for compressible flows, Mach number profiles have been computed and are given in Fig. 3. It is apparent that the Mach number is not uniform across the secondary flow, which decelerates toward the supersonic jet. This variation is entirely due to the static pressure variation since the total pressure is constant across the secondary flow. The static pressure increase toward the inner jet can be attributed to the free jet curvature which is imposed by the primary nozzle. It is worth noting that some radial profiles of axial velocity by Plumlee<sup>25</sup> clearly show the same feature.

Fan engine speeds have been translated into values of  $M_f$  by means of a calibration procedure where the local Mach number has been measured approximately at the center of the free jet. This value must then be taken as a mean rather than as a unique  $M_f$  characterizing the secondary flow.

## III. SCREECH FREQUENCY IN STATIC AND FLIGHT CONDITIONS

### A. Static case

The screech frequency evolution with jet Mach number under static conditions is shown in Fig. 4. Only Strouhal numbers associated with fundamental screech tones are displayed.

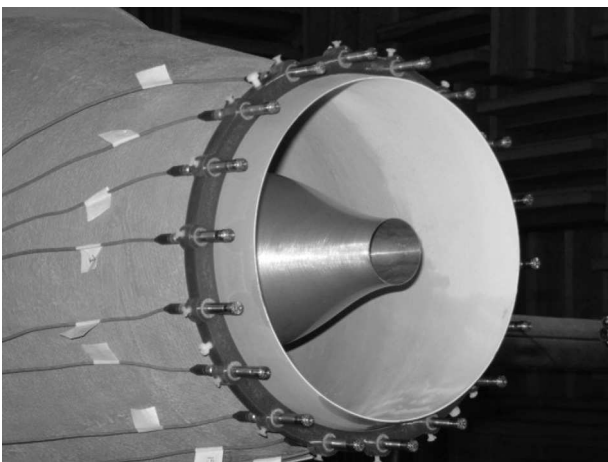


FIG. 2. The circular near field antenna used for screech mode study.

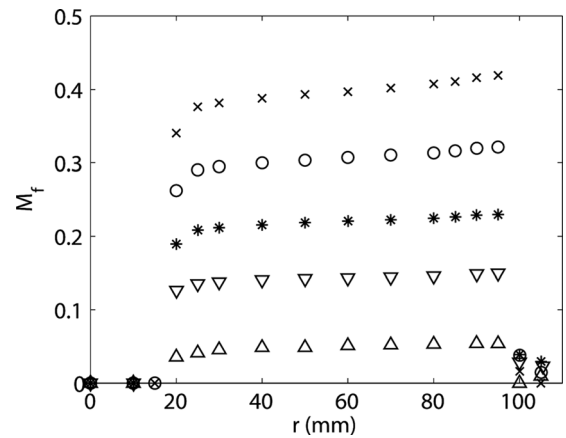


FIG. 3. Transverse profiles of local flight Mach number  $M_f$ , measured half a model jet diameter downstream of the exit. Fan engine speeds are denoted by the power supply related to its maximum value:  $\triangle$  11%,  $\nabla$  30.5%, \* 47%,  $\circ$  66%,  $\times$  86%. The primary jet (radial coordinate  $r < 19$  mm) is not operated ( $M_j = 0$ ).

The Strouhal number  $St_s$  is defined as  $f_s D / U_j$ , where  $f_s$  is the screech frequency and  $U_j$  the fully expanded jet velocity. The general Mach number dependence of screech frequency is very similar to the well known evolution, see, e.g., Powell *et al.*<sup>6</sup> Modes A1, A2, and B are clearly visible in Fig. 4. It is peculiar that the helical mode C is marginally dominant in our facility. Instead, a continuation of the flapping mode B was observed at higher  $M_j$ . This mode will be termed b in the following after the nomenclature of Powell *et al.*<sup>6</sup>

According to Powell's model,<sup>1</sup> adding up the time taken by flow disturbances to travel down one shock cell and the time needed by the acoustic waves outside the jet to propagate back the same period distance toward the nozzle gives the screech temporal period  $T_s$ ,

$$T_s = L_s / U_c + L_s / c_0, \quad (1)$$

with  $L_s$  the shock cell length,  $U_c$  the convection velocity of vortical disturbances in the mixing layer, and  $c_0$  the speed of sound outside the jet. Equation (1) leads straightforwardly to the expression of the screech frequency  $f_s$ ,

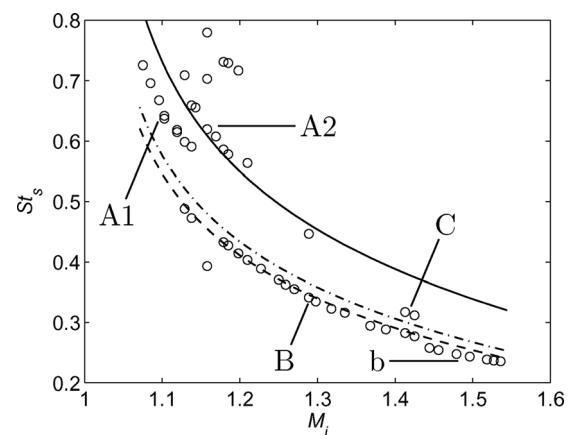


FIG. 4. Measured  $St_s$  against  $M_j$ ,  $M_f = 0$ . — Eq. (4), mode A2; -- Eq. (6), mode B; and - · - Eq. (5), mode C.

$$f_s = U_c/[L_s(1 + M_c)], \quad (2)$$

where the convective Mach number  $M_c$  denotes  $U_c/c_0$ . Essentially, the same formula is obtained by Tam *et al.*<sup>5</sup> Depending on the retained expressions for  $L_s$  and  $U_c$  as a function of  $M_j$  and jet total temperature  $T_t$ , many final expressions for  $f_s$  have been proposed. The evolution of  $L_s$  with  $M_j$  has generally been expressed as a function of  $\beta D$ , with  $\beta = (M_j^2 - 1)^{1/2}$ . The convection velocity is written as a fraction of the jet fully expanded velocity  $U_j$ , and  $U_c = 0.7 U_j$  seems to be the most usual value. However, Panda *et al.*<sup>26</sup> found a significant dependence of convection velocity with screech mode for a circular nozzle.

In Tam *et al.*,<sup>5</sup> the frequency expression was rewritten to express  $f_s D_j / U_j$  as a function of  $M_j$  and  $T_t$  only as

$$\frac{f_s D_j}{U_j} = \frac{0.67}{(M_j^2 - 1)^{1/2}} \left[ 1 + 0.7 M_j \left( 1 + \frac{\gamma - 1}{2} M_j^2 \right)^{-1/2} \left( \frac{T_{\text{amb}}}{T_t} \right)^{-1/2} \right]^{-1}. \quad (3)$$

In Eq. (3),  $D_j$  is the fully expanded jet diameter,  $T_{\text{amb}}$  the ambient temperature, and  $\gamma$  the ratio of specific heats. Massey and Ahuja<sup>24</sup> proposed two different screech formulae for modes A and C, starting from Eq. (3) and using specific  $U_c$  estimates for each mode. Also, it was noticed that a  $(M_j^2 - 1)^{1/3}$  dependence of shock spacing allowed a better fit of the experimental data. In this reference,  $f_s$  for mode A (axisymmetric) is written as

$$\frac{f_s D_j}{U_j} = 1.25 \frac{0.63}{1.1(M_j^2 - 1)^{1/3}} \left[ 1 + 0.63 M_j \left( 1 + \frac{\gamma - 1}{2} M_j^2 \right)^{-1/2} \left( \frac{T_{\text{amb}}}{T_t} \right)^{-1/2} \right]^{-1}, \quad (4)$$

and for mode C (helical) as

$$\frac{f_s D_j}{U_j} = \frac{0.615}{1.1(M_j^2 - 1)^{1/3}} \left[ 1 + 0.615 M_j \left( 1 + \frac{\gamma - 1}{2} M_j^2 \right)^{-1/2} \left( \frac{T_{\text{amb}}}{T_t} \right)^{-1/2} \right]^{-1}. \quad (5)$$

The following expression is proposed for mode B, which was left out by Massey and Ahuja:<sup>24</sup>

$$\frac{f_s D_j}{U_j} = \frac{0.58}{1.12(M_j^2 - 1)^{1/3}} \left[ 1 + 0.58 M_j \left( 1 + \frac{\gamma - 1}{2} M_j^2 \right)^{-1/2} \left( \frac{T_{\text{amb}}}{T_t} \right)^{-1/2} \right]^{-1}, \quad (6)$$

where the value of the convection velocity  $U_c = 0.58 U_j$  is taken from Panda *et al.*<sup>26</sup> for mode B.

The Strouhal numbers  $St_s = f_s D / U_j$  computed from these expressions are superimposed on our measured values in Fig. 4. It can be seen that the agreement is good for all modes. The formula of Massey and Ahuja<sup>24</sup> for mode A seems in particular to be calibrated for mode A2. Equation (5) is in fair agreement with the two higher frequency points around  $M_j = 1.4$ , confirming that the helical mode is marginally present in our facility. Finally, Eq. (6) follows closely the measured frequencies for mode B over a large  $M_j$  range, giving support to the  $(M_j^2 - 1)^{1/3}$  dependence of shock spacing proposed by Massey and Ahuja.

## B. Flight configuration

In the following, results for screech modes A1, A2, B, and b in flight are presented. For a given mode, only one jet Mach number is here considered, being representative of the main features noticed by the authors for the corresponding mode. Jet Mach numbers of 1.10, 1.15, 1.35, and 1.50 have thus been selected. For these values of  $M_j$ ,  $M_f$  has been gradually varied from 0 to about 0.4 upward and downward. The resulting screech frequencies are displayed in Fig. 5 (the labels in Fig. 5 are associated with the analysis developed in Sec. IV). The general trend is a decrease of screech frequency with  $M_f$ . In all cases and especially for  $M_j = 1.15$ , the frequency evolution is discontinuous. Finally, some frequency jumps are seen to give rise to hysteretical behaviours, insofar as the upward and downward frequency curves are not always superimposed. The screech frequency prediction in flight is now discussed.

The screech frequency prediction formula has been extended to forward flight by Hay and Rose<sup>10</sup> and later by Bryce and Pinker,<sup>13</sup> starting from Powell's<sup>1</sup> static expression. The only modification of the expression of the screech time period in flight as compared to Eq. (1) arises from the slowed acoustic propagation back toward the nozzle,

$$T_s = L_s / U_c + L_s / (c_0 - U_f), \quad (7)$$

where  $U_f$  is the flight velocity. This leads to

$$f_s = U_c / (L_s [1 + M_c / (1 - M_f)]). \quad (8)$$

Equation (8) is also the same as that given by Tam.<sup>11</sup> Here again, the relevant expressions for  $L_s$  and  $U_c$  can be discussed. First, the importance of considering the shock cell lengthening for frequency prediction was already underlined by Norum and Shearin.<sup>14</sup> Morris<sup>27</sup> proposed an expression for the shock cell length in flight from a vortex sheet model with proper boundary conditions. The model prediction for  $M_j = 1.50$  is shown in Fig. 6 along with some mean shock cell length measurements from schlieren recordings of the present study. Also displayed are estimates from static pressure profiles of Norum and Shearin<sup>28</sup> for  $M_j = 1.49$ . The agreement between the theory and the present results is seen to be good, especially considering the dispersion in the

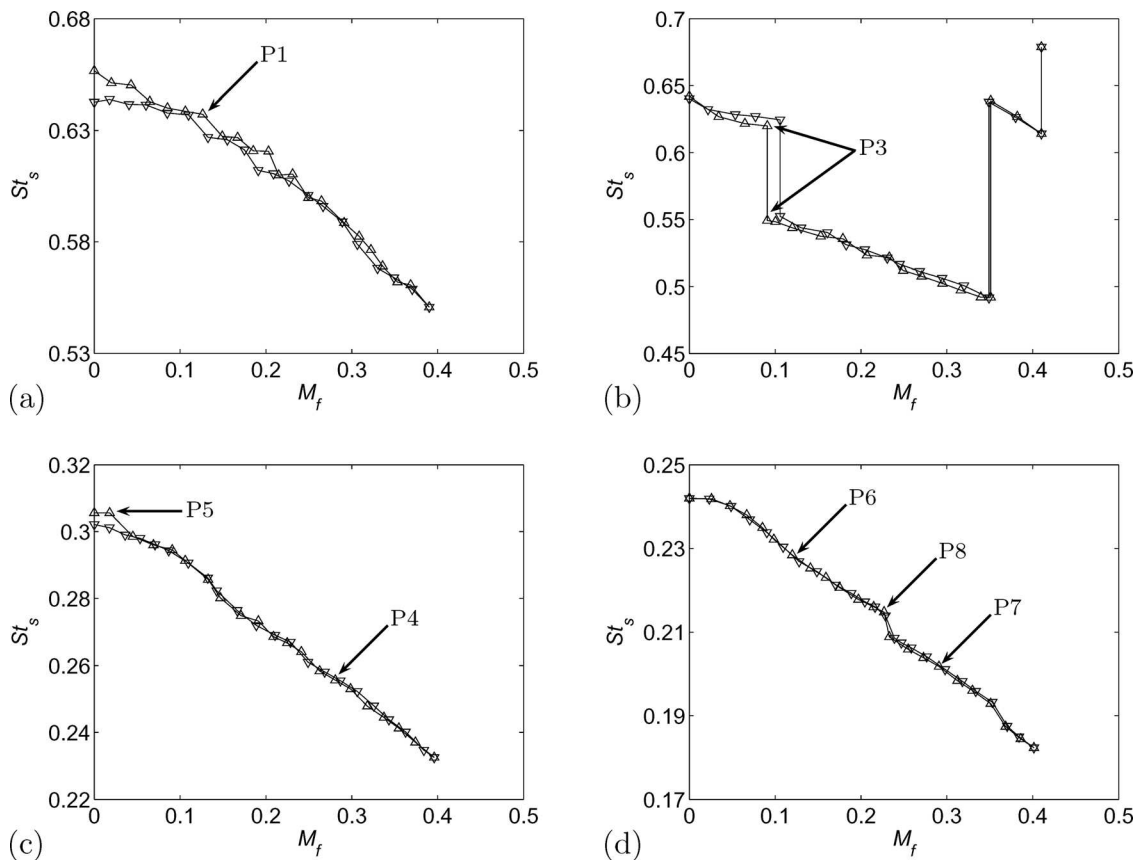


FIG. 5. Evolution of  $St_s$  with flight Mach number. (a) Mode A1,  $M_j=1.10$ ; (b) mode A2,  $M_j=1.15$ ; (c) mode B,  $M_j=1.35$ ; and (d) mode b,  $M_j=1.50$ .  $\triangle$  upward evolution of flight velocity;  $\nabla$  downward evolution of flight velocity.

experimental data. Hence, the theoretical expression from Morris<sup>27</sup> is used in the following.

The convection velocity can be calculated as

$$U_c = \alpha(U_j - U_f) + U_f \quad (9)$$

by generalizing Bryce and Pinker's formula,<sup>13</sup> who use  $\alpha=0.7$ . The value of  $\alpha$  is considered here to be specific to each screech mode, according to the measurements of Panda

*et al.*<sup>26</sup> On the other hand, the study of Sarohia and Massier<sup>29</sup> suggests that the boundary layer on the engine cowl, or for us on the outer wall of the model jet nozzle, shields the model jet from the secondary flow. As a result, the relevant scale velocity is expected to be  $U_j$  and not  $U_j - U_f$ . Hence, according to this hypothesis,

$$U_c = \alpha U_j, \quad (10)$$

where  $\alpha$  takes on the same values as in Eq. (9). The two prediction formulae for  $f_s$  derived from these expressions for  $U_c$  have been tested against the measured screech frequency evolutions displayed in Fig. 5 for the two higher Mach number cases. The results are depicted in Fig. 7, for  $\alpha=0.58$  coming from Panda *et al.*<sup>26</sup> and  $L_s$  provided by Morris' model.<sup>27</sup> Equation (10) leads to a better prediction of the slope of  $St_s$  with  $M_f$ . The agreement is even found to be very good for both  $M_j$  if one matches the predicted Strouhal number to the measured one at  $M_f=0$ . This would support the hypothesis of Sarohia and Massier.<sup>29</sup>

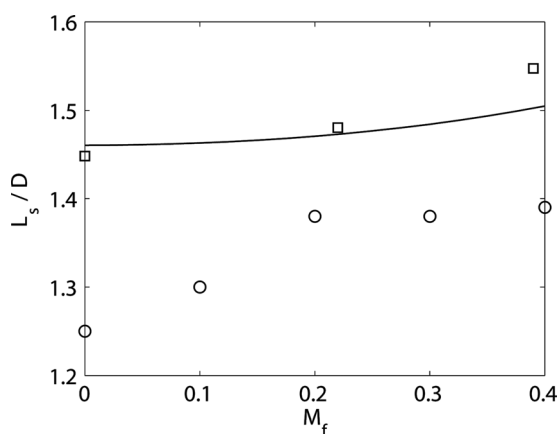


FIG. 6. Shock cell length  $L_s$  normalized by the nozzle diameter  $D$  as a function of  $M_f$ .  $\square$  present study,  $M_j=1.50$ ;  $\circ$  Norum and Shearin,<sup>28</sup>  $M_j=1.49$ ; — Morris' model.<sup>27</sup>

#### IV. ANALYSIS OF NEAR FIELD MICROPHONE SIGNALS

In addition to allowing screech frequency predictions to be established, the time signals have also been used to investigate the modal behaviour of screech in flight. Several analyses have been performed.

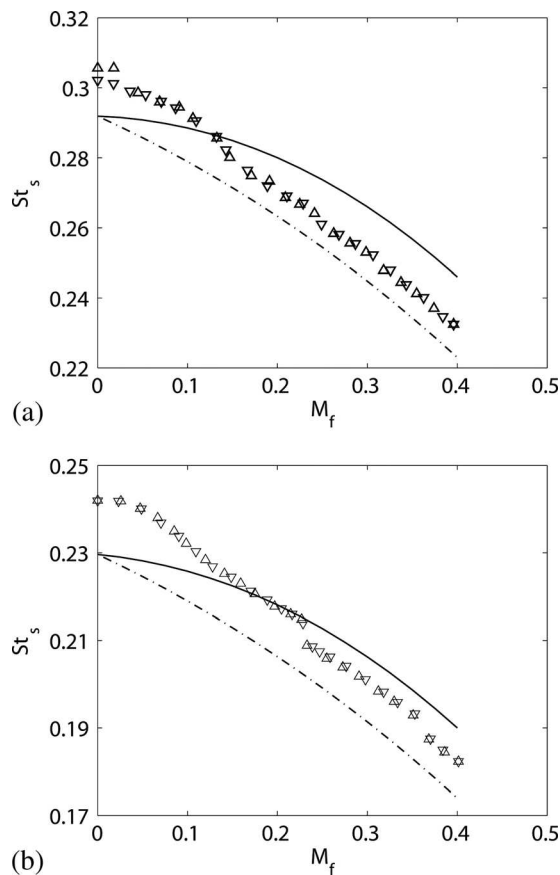


FIG. 7. Prediction of screech frequency in flight by Eq. (8). (a)  $M_j = 1.35$ ; (b)  $M_j = 1.50$ .  $L_c$  is computed as in Morris.<sup>27</sup>  $\Delta$ ,  $\nabla$  measurements, —  $U_c = 0.58(U_j - U_f) + U_f$ , and - - -  $U_c = 0.58 U_j$ .

For the sinuous mode B, the azimuthal distribution of acoustic pressure in the near field is antisymmetric with respect to a plane containing the jet axis. Next to this plane, the screech amplitude is vanishing, whereas it is maximum in the direction normal to the plane. Moreover, this plane is known to slowly rotate.<sup>6</sup> Using the near field azimuthal microphone antenna (Fig. 2), this behaviour can be followed by tracking the azimuthal location of the microphones associated with the lowest root mean square pressure calculated over a small number of screech periods, namely, ten in the results presented here. In the following, the position of the plane of antisymmetry is located by its azimuthal angle  $\phi_p$ , as defined in Fig. 8.

Additionally, the time evolution of phase relationships between the microphones has been estimated. One near field microphone has been chosen as phase reference, and its azimuthal angle has been arbitrarily taken as  $\phi_m = 0^\circ$ . For each of the remaining microphones, the phase angle difference to the reference microphone has been computed from the time delay yielding the maximum cross-correlation between the two time signals. Time extracts of ten screech periods have been considered to evaluate an instantaneous phase relation. Repeating the calculation for such temporal blocks over the whole recording has allowed the time evolution of phase differences to be determined. The phase relations, written  $\Delta\psi$ , are expressed as a fraction of screech period. Thus,  $\Delta\psi = 0$

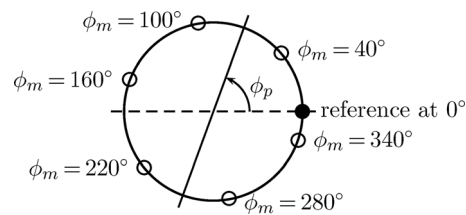


FIG. 8. Sketch of the near field azimuthal microphone antenna, defining the location of microphones as a function of the azimuthal angle  $\phi_m$ , and showing a possible location for the plane of antisymmetry, denoted by  $\phi_p$  (relevant for flapping modes only).

means that the signals are in phase, while  $\Delta\psi = \pm 0.5$  stands for an opposite phase relation. In the following, only a limited number of near field microphones is considered, to enhance the readability of the displayed results. Their position is shown in Fig. 8.

Finally, the modal detection method by Massey and Ahuja<sup>24</sup> has been implemented and used to check some of the time results. A measure of the modal amplitude associated with each azimuthal mode contained in the time signals is obtained. Contrary to the first two techniques, this one has been used on the entire time signals and has thus provided integrated information over the whole recordings. In the following, the azimuthal order is written  $m$ .

Before applying the first two processings, the time signals have been digitally filtered around the screech frequency. It not only yields a more suitable frame for postprocessing, but also ensures that the dominant screech frequency is selected for analysis in the case of multiple screech tones. The points investigated specifically in the following are labeled on the frequency plots of Fig. 5 and described in Table I.

### A. Mode A1

The case of  $M_j = 1.10$  is discussed now. The screech Strouhal number evolution against  $M_f$  is shown in Fig. 5(a) and some small discontinuities can be identified. The first one occurring around  $M_f = 0.13$  is considered here. A time trace of P1 is shown in Fig. 9(a). All microphones are seen to be in phase on this sample. The modal detection (b), which is an integrated result over the one-second recording, confirms that the axisymmetrical mode  $m = 0$  dominates over the helices  $m = \pm 1$ . Phase relation calculations for all the other points have been performed, and the microphone

TABLE I. Description of the points specifically studied in Sec. IV. In all cases, the experimental points for ascending  $M_f$  are considered.

Point name	$M_j$	$M_f$
P1	1.10	0.13
P3	1.15	0.09
P4	1.35	0.28
P5	1.35	0.02
P6	1.50	0.12
P7	1.50	0.29
P8	1.50	0.23

signals have always been seen to be in phase. This allows us to conclude that the screech at  $M_j = 1.10$  remains axisymmetric at all  $M_f$  values, in spite of the frequency jumps.

## B. Mode A2

The mode A2, which is dominant at  $M_j = 1.15$ , corresponds to the only fully expanded jet Mach number investigated that shows strong frequency jumps, see Fig. 5(b). It seems interesting to note that at  $M_f = 0$  already, several non-harmonically related screech frequencies are visible in Fig. 4, indicating an unstable behaviour also pointed out by Davies and Oldfield.<sup>4</sup> The presence of several screech frequencies is maintained throughout the  $M_f$  range tested. This is obvious on the map of sound pressure level versus flight Mach number displayed in Fig. 10. The dominant screech frequency at each value of  $M_f$  is the one selected for the plot of Fig. 5(b). Point P3, corresponding to the first jump, is examined here. A time-frequency diagram built on the two-second time signal is shown in Fig. 11(a). The two screech frequencies visible on each side of the jump are seen to appear alternatively. A phase analysis has been applied to the time signals, pass-band filtered around the upper screech frequency in Fig. 11(b) and around the lower one in Fig. 11(c).

It should be noted that the calculated phase relations  $\Delta\psi$  can only take discrete values due to the time signal discreti-

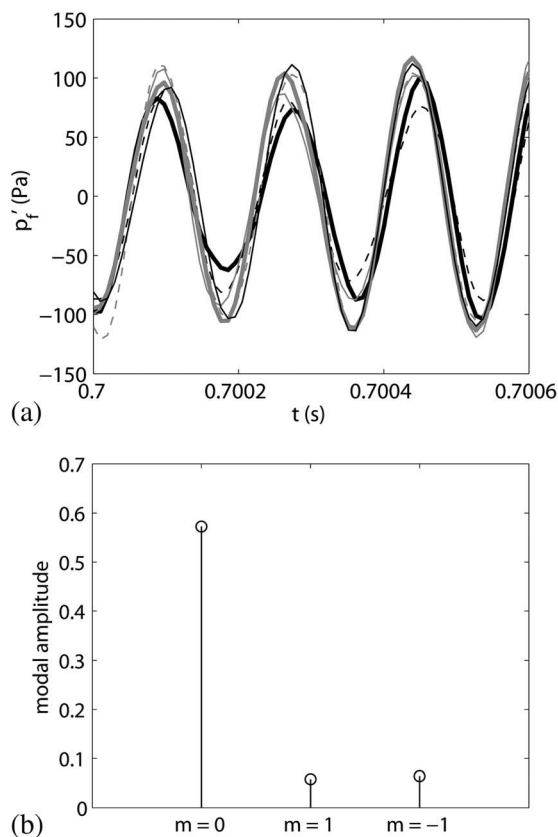


FIG. 9. Mode A1,  $M_j = 1.10$ , point P1: (a) time signals; (b) modal content. —  $\phi_m = 40^\circ$ , —  $\phi_m = 100^\circ$ , — (gray)  $\phi_m = 160^\circ$ , —  $\phi_m = 220^\circ$ , — (gray)  $\phi_m = 280^\circ$ , —  $\phi_m = 340^\circ$ .  $p'_f$  is the filtered near field pressure and  $t$  denotes time.

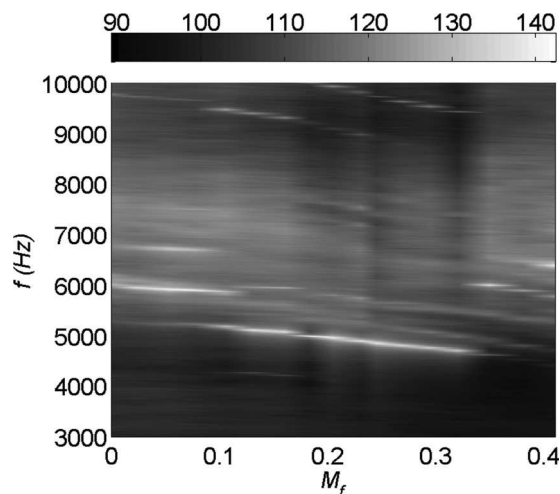


FIG. 10. Mode A2,  $M_j = 1.15$ . Map of sound pressure level (SPL) against  $M_f$ . The colorbar codes SPL in dB/Hz.

zation. The resolution is  $f_s/f_{acq}$ , where  $f_{acq}$  is the sampling rate. For the case in Fig. 11(b),  $f_s/f_{acq} = 0.057$ , which explains that the displayed phase relations are not quite smooth.

One clearly remarks that, when the signals are pass-band filtered around a given frequency  $f_s$ , the phase  $\Delta\psi$  is equal to zero when this frequency dominates in the time-frequency diagram: all microphones are approximately in phase at both frequencies, suggesting that both screech modes are axisymmetric. In fact, it is so for all the flight Mach numbers investigated at this value of  $M_j$ . The second and third jump visible in Fig. 5(b) do not reveal any other type of mode. It means that the mode switching when  $M_j$  is increased is like the one between modes A1 and A2 for static jets: there is no change of azimuthal mode dominance. It seems from Fig. 10 that all encountered axisymmetric modes are present at most values of  $M_f$  and that they are alternatively emphasized as  $M_f$  is varying. Flight is known to modify the jet mixing layer stability,<sup>30</sup> and for this value of  $M_j$ , already showing multiple stages at  $M_f = 0$ , the most amplified mode is seen to vary with  $M_f$ .

## C. Mode B

A plot of phase relations for point P4 of sinuous mode B is shown in Fig. 12, along with an extract from the time signals. The flapping property of this mode stands out quite clearly, since the microphones can be gathered into two groups which are in opposite phase relation. It can be inferred from Fig. 12 that the plane of antisymmetry lies between  $100^\circ$  and  $160^\circ$ , as shown by the sketch of the near-field antenna drawn on the figure. This feature holds throughout the whole flight Mach number range; the screech at this value of  $M_j$  is thus always flapping.

Nevertheless, one flight effect on the rotation of the plane of antisymmetry has been identified. The position of the plane against time is shown in Fig. 13(a) for P5, over 0.5 s. It can be seen that the plane of antisymmetry completes approximately six half-rotations within 0.5 s. In Fig. 13(b), a

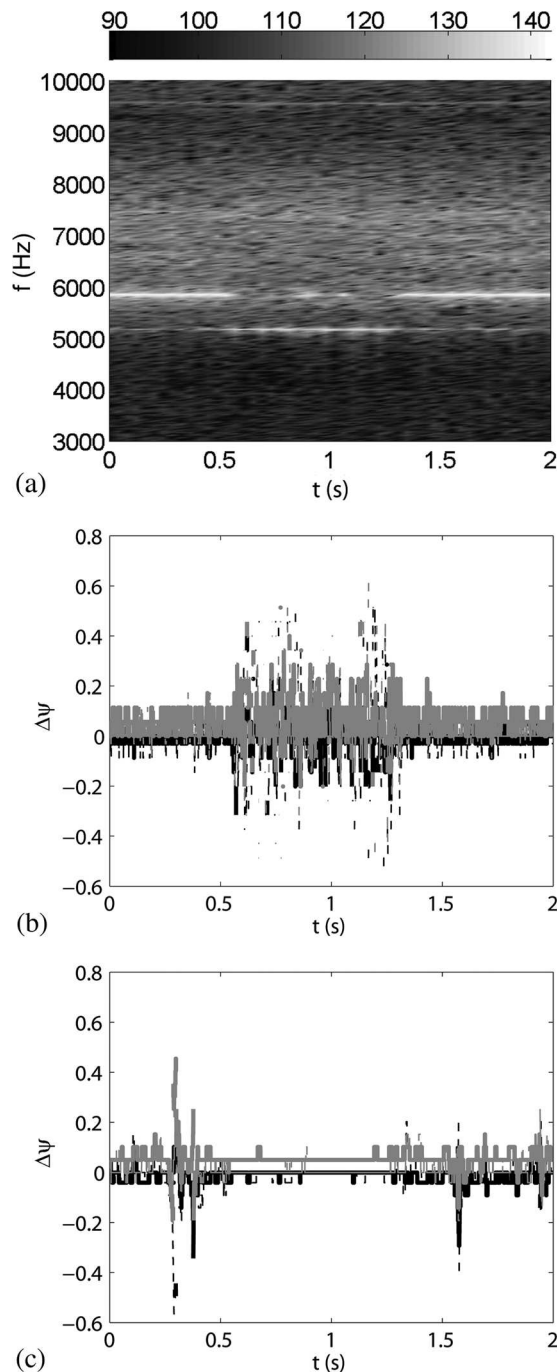


FIG. 11. Mode A2,  $M_j = 1.15$ , point P3: (a) time-frequency diagram (the colorbar codes SPL in dB/Hz); (b) phase relations  $\Delta\psi$  against time for the upper screech frequency,  $f_s = 5841$  Hz; (c)  $\Delta\psi$  against time for the lower screech frequency,  $f_s = 5171$  Hz. —  $\phi_m = 40^\circ$ , - -  $\phi_m = 100^\circ$ , — (gray)  $\phi_m = 160^\circ$ , —  $\phi_m = 220^\circ$ , — (gray)  $\phi_m = 280^\circ$ , - -  $\phi_m = 340^\circ$ .

focus around the screech frequency of the spectrum at P5 is displayed. Two distinct peaks are readily identified. Their frequencies are 3236 Hz and 3248 Hz, which means that they are 12 Hz apart. Now there are six plane half-rotations over the first half-second of the time recording, which is connected to this 12 Hz difference in the way highlighted next. The modal detection algorithm has been applied on those two frequencies. Azimuthal modes  $m = -1$  and  $m = +1$  are seen to dominate separately for each frequency. Independ-

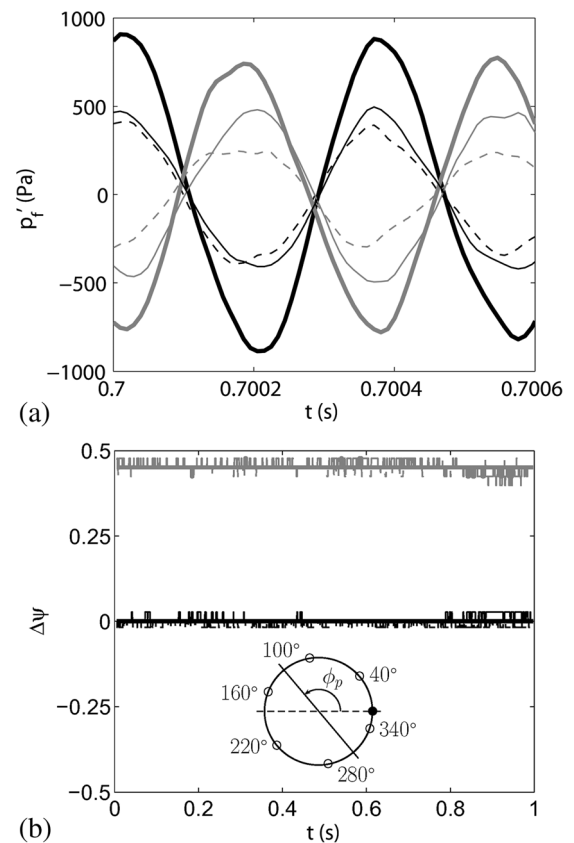


FIG. 12. Mode B,  $M_j = 1.35$ , P4. (a) Time signals; (b) phase relations  $\Delta\psi$  against time. —  $\phi_m = 40^\circ$ , - -  $\phi_m = 100^\circ$ , — (gray)  $\phi_m = 160^\circ$ , —  $\phi_m = 220^\circ$ , — (gray)  $\phi_m = 280^\circ$ , - -  $\phi_m = 340^\circ$ . The insert in (b) displays the approximate location of the plane of antisymmetry.

ently, if one adds up two artificial time signals of azimuthal modes  $m = -1$  of frequency  $f_1$  and  $m = +1$  at  $f_2$ , it is seen that a flapping mode results but with a plane of antisymmetry rotating at  $|f_1 - f_2|$ . To conclude, it is believed that the existence of two counter-rotating helices of different frequencies is responsible for the rotation of the plane of antisymmetry visible for P5.

Now, the first two points in Fig. 5(c) at low  $M_f$  are seen to have rotating planes in connection with several spectral peaks very close to each other. As of the third point, from  $M_f = 0.05$  upward, only one peak frequency is visible in the spectra, which is associated with a steady plane of antisymmetry. It is concluded that the secondary flow stabilizes the screech at  $M_j = 1.35$  in some way. Furthermore, while  $M_f$  is decreased to zero, mode B remains stable even at vanishing flight Mach number. So, once the screech has been stabilized, it seems to remain stable even in the absence of flight. This change of state between upward and downward variations of  $M_f$  most probably explains the frequency difference noticed between both cases at  $M_f = 0$  (see Fig. 5(c)).

#### D. Mode b

The upper fully expanded Mach number investigated is  $M_j = 1.50$ . The screech frequency evolution in flight is given in Fig. 5(d) and a small jump occurs around  $M_f = 0.23$ . The

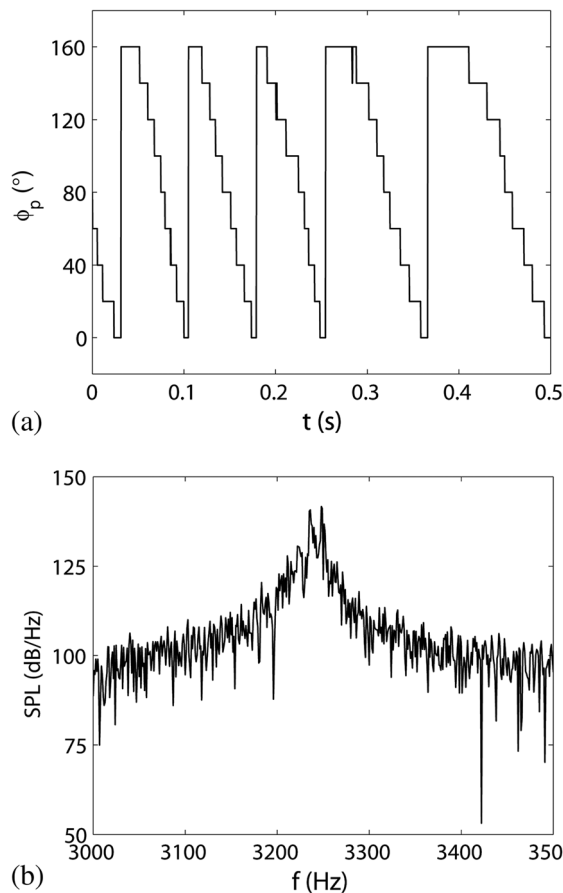


FIG. 13. Mode B,  $M_j=1.35$ , P5. (a) Azimuthal position of the plane of antisymmetry against time; (b) focus around the screech frequency of the spectrum.

phase relations for P6 on one side of the jump and P7 on the other side are shown in Fig. 14. This mode is obviously flapping as the same phase relations as for mode B are visible. As for mode A2, the frequency jump does not change the dominant azimuthal modes. Incidentally, these results confirm that this upper screech mode is, indeed, a mode b as it was stated earlier, and not a helical mode C.

Point P8 is nevertheless worth mentioning. This recording is the one right before the screech frequency jumps to lower frequencies. The position of the rotating plane of antisymmetry is shown in Fig. 15 over a short time period extracted from the 1-s recording, while the phase relations are displayed in Fig. 16(a) over the same time interval. Moreover, the entire time traces (not shown here) very much look like the ones shown by Powell *et al.*<sup>6</sup> in their Fig. 15(a), revealing rapid and strong amplitude modulations over time. The plane rotation and the phase relation design are both fully stationary throughout the whole recording. The phase relation pattern looks rather puzzling at first sight but it has been artificially reconstructed in the following manner. First, as indicated by Fig. 15, the plane completes approximately forty half-rotations in a second. Furthermore, a second frequency peak of lower amplitude located 41 Hz aside the dominant one is visible in the acoustic spectra (not shown here). The modal content of the acoustic near field, determined using the modal detection algorithm, is exclusively

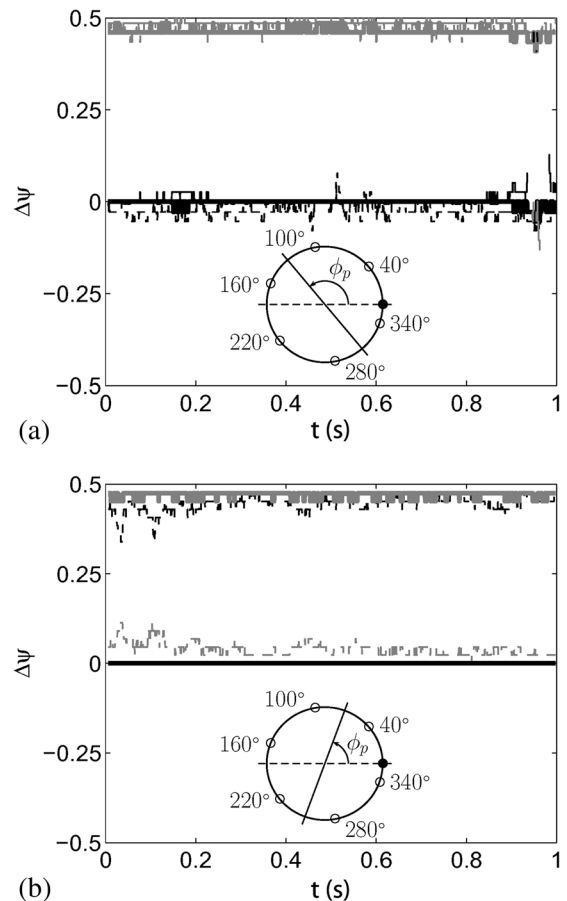


FIG. 14. Phase relations  $\Delta\psi$  against time. Mode b,  $M_j=1.50$ . (a) P6; (b) P7. —  $\phi_m=40^\circ$ , —  $\phi_m=100^\circ$ , — (gray)  $\phi_m=160^\circ$ , —  $\phi_m=220^\circ$ , — (gray)  $\phi_m=280^\circ$ , —  $\phi_m=340^\circ$ . The inserts display the approximate location of the plane of antisymmetry.

$m=-1$  at the screech frequency and  $m=+1$  at the other peak frequency. It seems then that two helical modes of separate frequency coexist, in the manner of what happens for point P5. Analytically, a time signal was built as the sum of such two helices, whose orientations are opposite, frequencies are given by the acoustic spectra, and amplitudes are obtained by filtering the time signals sharply around each peak frequency and noting the amplitude of the resulting

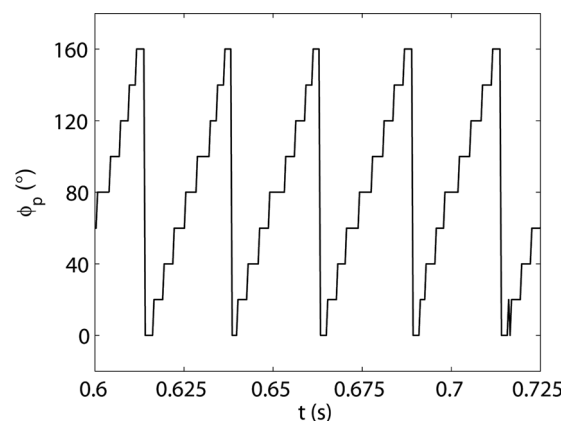


FIG. 15. Mode b,  $M_j=1.50$ , P8: location of the plane of antisymmetry over one eighth of a second.

signal. The ratio of these two amplitudes is the relevant parameter to properly reconstruct the time signals. Finally, the phase relations for the artificial signals made up of both helices have been computed, and the pattern shown in Fig. 16(b) has been obtained. It is obviously the same pattern as the experimental counterpart. The screech at P8 is thus made up of two counter-rotating helices of different frequencies and amplitudes. It has been observed that this peculiar behaviour builds up from the three previous points while  $M_f$  is increased and completely vanishes just after the jump. In addition, the agreement between measured and reconstructed phase relations demonstrates the adequacy of the phase relation analysis.

Finally, the current point P8 is then rather similar to P5 studied above. The main differences are a perfectly constant angular speed of the plane rotation at P8 which makes it particular among all the investigated points and the amplitude difference between the two counter-rotating helices. The latter property is responsible for the peculiar phase relation pattern, which has not been seen on any other measured point.

### C. Summary of the time signal analyses

Our results are summarized in Table II. The expression *double helical* denotes the configuration where screech is

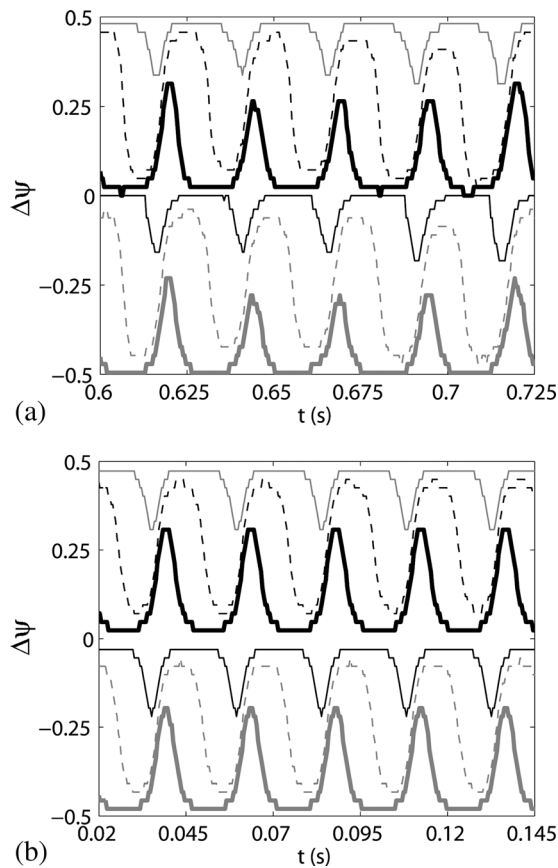


FIG. 16. (a) Mode b,  $M_j = 1.50$ , P8: phase relations between the recorded pressure signals over one eighth of a second. (b) Reconstruction of the phase relations for a time signal containing:  $m = +1$  at a frequency  $f = 2462$  Hz and an amplitude of 1200 Pa;  $m = -1$  at a frequency  $f = 2421$  Hz and an amplitude of 800 Pa. —  $\phi_m = 40^\circ$ , —  $\phi_m = 100^\circ$ , — (gray)  $\phi_m = 160^\circ$ , —  $\phi_m = 220^\circ$ , — (gray)  $\phi_m = 280^\circ$ , —  $\phi_m = 340^\circ$ .

TABLE II. Conclusions of the time signal analyses performed.

$M_j$	$M_f$			
	0	Low	Moderate	High
1.10	Mode A1	Mode switching between axisymmetric modes		
1.15	Mode A2	Mode switching between axisymmetric modes		
1.35	Mode B	Double helical $\rightarrow$ flapping Flapping $\leftarrow$ flapping		
1.50	Mode b	Flapping $\leftrightarrow$ double helical $\leftrightarrow$ flapping		

made up of two counter-rotating helices of different frequencies, which makes the plane of antisymmetry rotate. The wording *flapping* denotes as usual a screech with two counter-rotating helices of same frequency. The frequency discontinuities, indicating some kind of mode switching, have never been related to a change in the azimuthal mode content of screech. This does not mean, however, that such a switch is impossible. Actually, it has already been reported by Norum and Shearin.<sup>14</sup> Values of  $M_j$  located near a natural mode switching under static conditions might give rise to such azimuthal mode changes in flight condition.

## V. FLIGHT EFFECTS ON SCREECH AMPLITUDE

### A. Far field acoustic results

One well-known disadvantage of free jet facilities to simulate flight conditions is the presence of the external shear layer between secondary jet and quiescent medium,

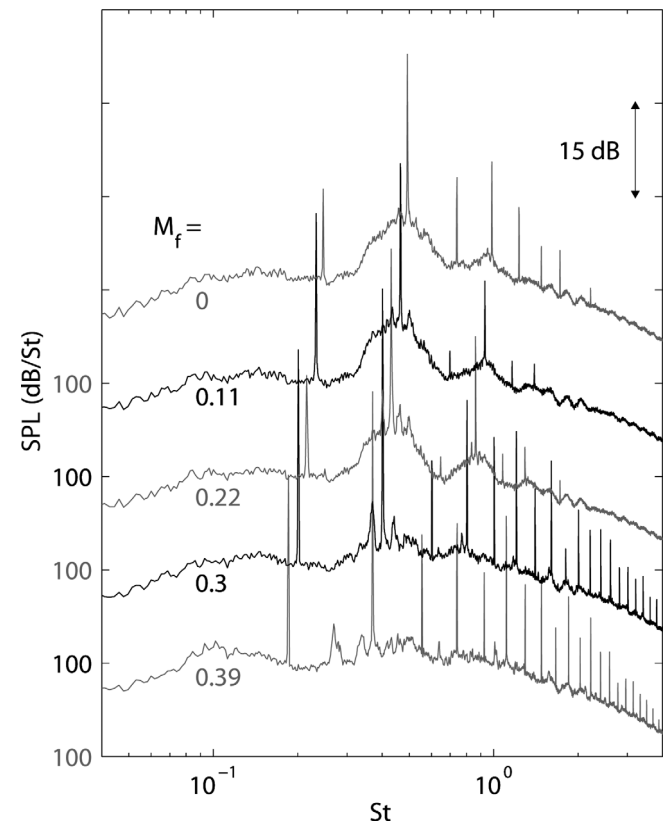


FIG. 17. Far field acoustic spectra in dB/St, with  $St = fD/U_j$ .  $M_j = 1.50$ ,  $M_f = 0, 0.11, 0.22, 0.30, 0.39$ , and  $\theta_e = 90^\circ$ .

which does not exist in a real flight configuration and whose influence on the radiated sound waves must be removed for the analysis of far field measurements. Many studies were devoted to this issue and the correction procedures, consisting of angle and amplitude corrections, are now widely accepted. The angle correction used in this work comes from Amiet<sup>31,32</sup> and is the same as the one developed by Ahuja *et al.*<sup>33</sup> Spectra at equal emission polar angle  $\theta_e$  are compared since this angle should reflect source changes due to flight and not spectral modifications due to propagation effects. Amiet's amplitude correction for a cylindrical shear layer<sup>32</sup> has also been implemented. The correction to equal distance from the present source position has been retained, *not* the correction to equal distance from what is referred to as the retarded source position in this reference. No account has been taken for the actual source position, which is supposed to be the nozzle exit for angle and amplitude corrections.

The cases  $M_j = 1.10, 1.35,$  and  $1.50$  are investigated. According to Sec. IV, these values of  $M_j$  correspond to modes A1, B, and b, respectively. A2 is not included because of the significant flight induced mode switches reported above, which could have made any comparison throughout the  $M_f$  range tentative. Only data for  $\theta_e = 90^\circ$  are shown. At this angle,  $\theta_e$  is very near the geometrical angle and amplitude corrections are small.  $\theta_e = 37.5^\circ$  and  $130^\circ$  have also been investigated and lead to the same conclusions as the ones presented here. All acoustic spectra are obtained by

averaging of 120 individual spectra with frequency resolution of 1 Hz. Some spectra for  $M_j = 1.50$  and  $\theta_e = 90^\circ$  are displayed in Fig. 17. It is already apparent that the screech is not reduced at high  $M_f$ , which is at odds with the conclusion of Viswanathan and Czech.<sup>17</sup> To the contrary, it seems rather enhanced as is visible from the number of harmonics that appear. In order to account for all harmonics, the far field spectra are analysed as follows. The OASPLs are computed. Then, the screech peaks are digitally removed, and the sound pressure level linearly interpolated over the defined narrow gaps. A screech free spectrum is thus built, whose OASPL is also calculated. From these two OASPLs, the sound pressure level associated with screech exclusively can be deduced by subtraction. This particular sound pressure level, noted  $SPL_s$ , contains the contribution of all screech harmonics, and its evolution with  $M_f$  shows directly the total screech energy dependence on flight Mach number. From the OASPL of the complete spectrum and  $SPL_s$ , the portion of the total acoustic energy coming from screech,  $p'_{rms}{}^s / p'_{rms}$ , ratio of root mean square screech fluctuating pressure to total fluctuating pressure, can ultimately be calculated. This procedure also presents the advantage of considering a possible widening of screech peaks which could arise from turbulence scattering by the external shear layer, as discussed in Schlinker and Amiet.<sup>34</sup> It is believed that the whole screech energy is thus considered, apart from what is lost by turbulence absorption through the external shear layer.

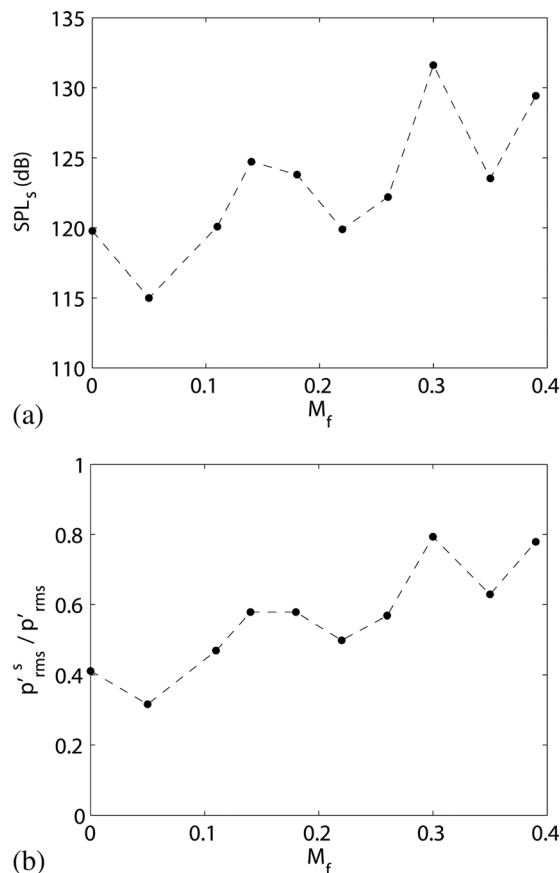


FIG. 18. (a) Evolution of screech sound pressure level with flight Mach number  $M_f$ ; (b) screech energy fraction against  $M_f$ .  $M_j = 1.50$  and  $\theta_e = 90^\circ$ .

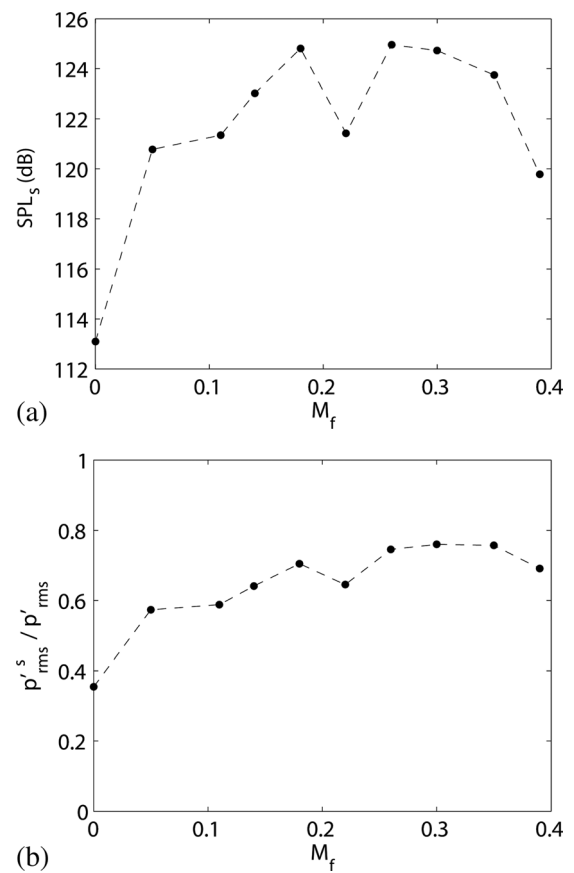


FIG. 19. (a) Evolution of screech sound pressure level with flight Mach number  $M_f$ ; (b) screech energy fraction against  $M_f$ .  $M_j = 1.35$  and  $\theta_e = 90^\circ$ .

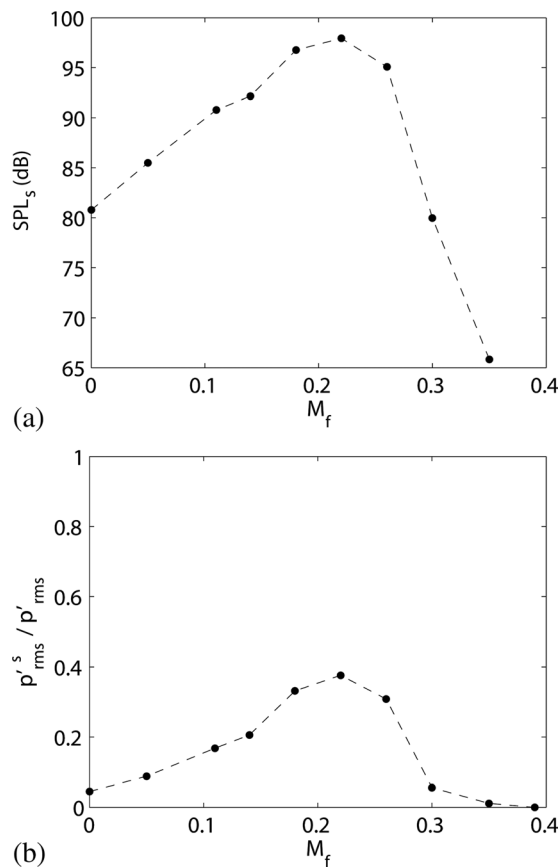


FIG. 20. (a) Evolution of screech sound pressure level with flight Mach number  $M_f$ ; (b) screech energy fraction against  $M_f$ .  $M_j = 1.10$  and  $\theta_c = 90^\circ$ .

Some results are shown in Fig. 18 for  $M_j = 1.50$ . The OASPLs have been computed for  $f > 500$  Hz to avoid considering the low frequency range where reflections could occur. Above this frequency, it was checked for all polar angles that the noise radiated by the external shear layer of the secondary flow is insignificant compared to the supersonic jet noise. Although the curves of Fig. 18 are not monotonous, the conclusion drawn from the spectra displayed in Fig. 17 is confirmed:  $SPL_s$  globally increases as  $M_f$  grows. Furthermore, the portion of acoustic energy coming from screech is also increasing and reaches about 0.8 above  $M_f = 0.3$ , which is twice the screech content at  $M_f = 0$ .

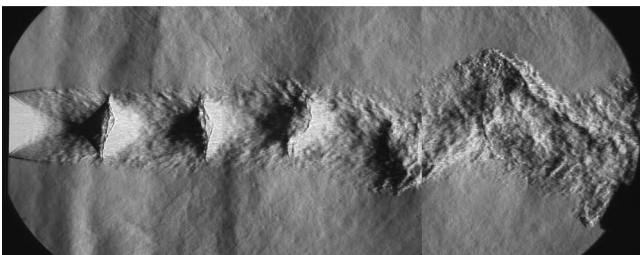


FIG. 21. Collage from three spark schlieren pictures of the supersonic jet plume, taken at three different times.  $M_j = 1.50$  and  $M_f = 0.39$ . Exposure time is  $6.7 \mu s$ .

The case  $M_j = 1.35$  is shown in Fig. 19. A global increase of  $SPL_s$  with  $M_f$  is also to be noted. The screech energy portion doubles between  $M_f = 0$  and 0.30. However, the levels drop slightly at the higher flight Mach numbers.

In the case  $M_j = 1.10$ , the cutoff frequency for computing the OASPLs had to be raised to 1500 Hz due to the lower model jet noise levels. Above it, the noise radiated by the external shear layer is at least 7 dB/Hz beneath the noise from the primary jet. Here, the conclusions are different from the two cases mentioned above, as shown in Fig. 20. While  $M_f$  is increasing, the screech is also enhanced but reaches maximal strength at  $M_f = 0.22$  before dropping and extinguishing at last at  $M_f = 0.39$ . Considering all the  $M_j$  cases analysed, one may conclude that there exists a  $M_f$ -limit for all  $M_j$  above which screech is finally reduced and that this limit increases with  $M_j$ . According to this hypothesis,  $M_f = 0.39$  would not be high enough for the screech levels at  $M_j = 1.50$  to fade out.

## B. Schlieren visualizations

The screech enhancement by flight Mach number at high  $M_j$  has also been identified through indirect effects of screech on the underexpanded jet dynamics. A collage made out of three spark schlieren images for the case  $M_j = 1.50$  and  $M_f = 0.39$  is shown in Fig. 21. The first shock is seen to be twisted within the jet plume, denoting a strong oscillation amplitude, and a large flapping motion of the jet occurs further downstream. These two features are now specifically investigated.

### 1. Shock oscillations with and without simulated flight

A shock tracking procedure has been developed by André *et al.*<sup>35</sup> and permits one shock to be followed from frame to frame in recorded schlieren movies. Here, the axial position of the tip of the first shock is followed in time. The power spectral density of this signal for  $M_j = 1.52$  and  $M_f = 0.39$  is given in Fig. 22 along with a far field acoustic spectrum recorded simultaneously. The former spectrum is computed from a one-second signal acquired at 29 000 Hz. The peak oscillation frequency is found to be exactly the

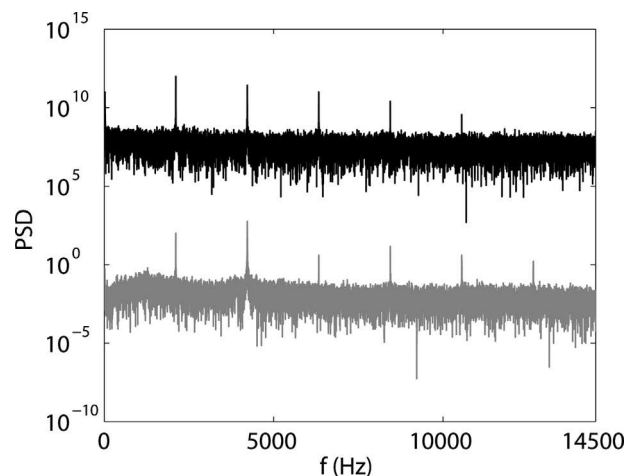


FIG. 22. Power spectral density (PSD) of one far field microphone signal at  $90^\circ$  to the jet axis (gray) and  $PSD \times 10^{10}$  of the signal containing the axial locations of the first shock tip for  $M_j = 1.52$  and  $M_f = 0.39$  (black).

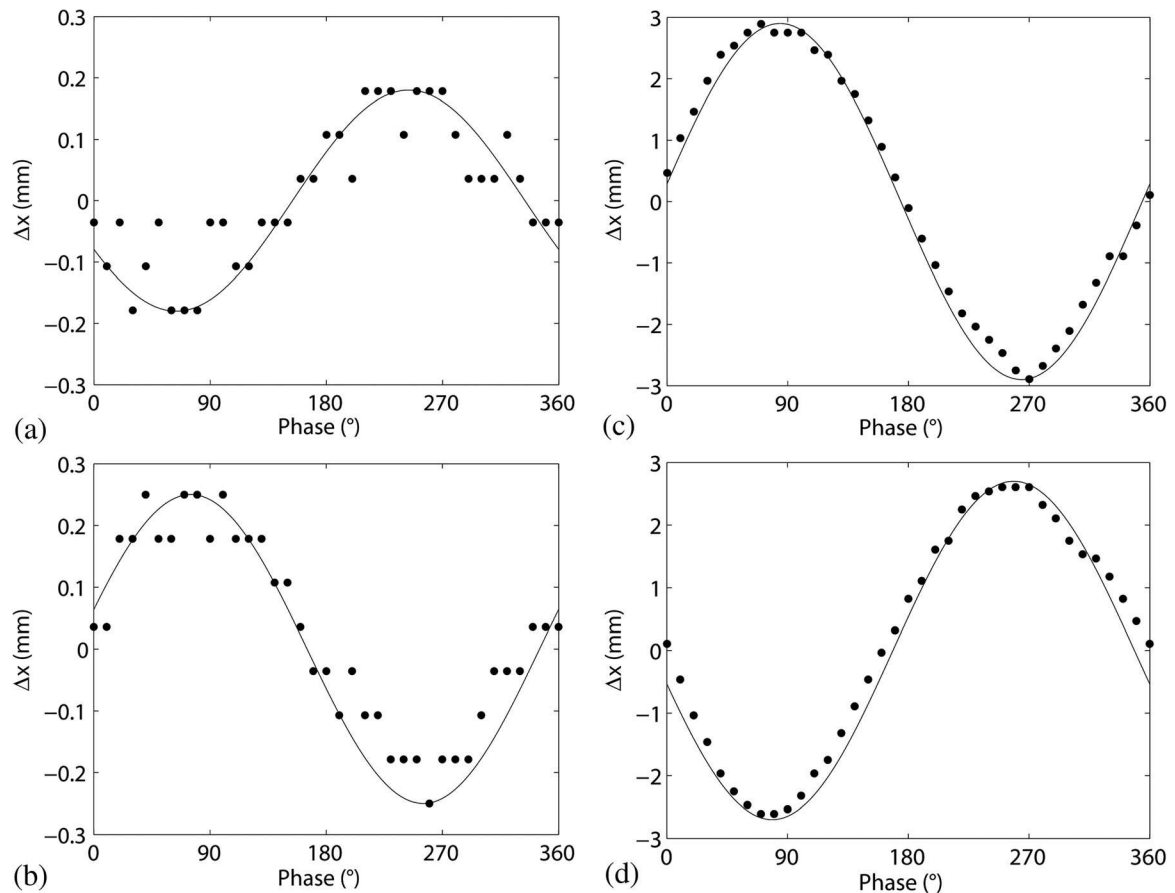


FIG. 23. Position of first shock ends in mm against screech phase,  $M_f = 1.52$ ; (a) upper tip,  $M_f = 0$ ; (b) lower tip,  $M_f = 0$ ; (c) upper tip,  $M_f = 0.39$ ; and (d) lower tip,  $M_f = 0.39$ . • shock positions as provided by the algorithm; — sinusoidal fit through the measured positions.

measured screech frequency. Even some harmonics are visible in the shock position spectrum. It confirms that the shock considered oscillates at the screech frequency. In order to estimate the oscillation amplitude, the schlieren images have been phase averaged and the same shock tracking procedure has been applied on the averaged pictures. The oscillations of the upper and lower tips of the first shock for  $M_f = 1.52$  and  $M_f = 0$  and  $0.39$  are shown in Fig. 23. Two conclusions may be drawn: (1) for each  $M_f$  value, the first shock oscillates antisymmetrically about the jet centreline, which corresponds to the flapping property of mode b; (2) the oscillation is greatly enhanced when the secondary flow is on. Indeed, the amplitude of oscillation goes from about 0.2 mm at  $M_f = 0$  to 2.8 mm at  $M_f = 0.39$ . As Panda's shock oscillation model<sup>36</sup> suggests that strong oscillation amplitudes come along with strong screech tones, these results are in agreement with the acoustic results reported above.

## 2. Jet large scale flapping motion

Sarohia *et al.*<sup>37</sup> reported a large scale lateral oscillation, also termed whipping motion, of the supersonic jet in simulated flight conditions. Other shadowgrams by Sarohia<sup>38</sup> clearly show this flow feature. Furthermore, Sarohia *et al.*<sup>37</sup> suppressed screech by inserting a rod inside the jet plume but could still observe the whipping motion, from which they inferred that it is not related to screech. Such a jet motion has also been observed under simulated flight

conditions in the present study, as it has been shown in Fig. 21. In this case, the oscillation amplitude, eight diameters downstream of the exit, has been roughly estimated to be of the order of one jet diameter. On the other hand, the application of the above mentioned tracking algorithm has permitted the oscillation frequency to be extracted, and it has been seen that the jet also flaps at the screech frequency, pleading for a connection between this motion and the tonal emission. With no flight velocity, however, no obvious flapping is visible although screech is present. Consequently, it could just as well be the screech enhancement by simulated flight which generates the strong whipping motion. This would corroborate the conclusion drawn from the far field acoustic results.

## VI. CONCLUSIONS

Flight effects on screech from an underexpanded supersonic jet have been experimentally investigated. Near field and far field acoustic measurements, supplemented by schlieren flow visualizations, have provided some insight into the behaviour of screech amplitude and frequency under flight conditions. The near field measurements have been performed with a circular azimuthal antenna mounted on the secondary nozzle.

The far field acoustic measurements have been analysed in a way that permits all the acoustic energy associated with screech to be considered, by including not only the fundamental tone but also the numerous harmonics. From

$M_j = 1.10$  to  $1.50$ , the screech is enhanced by forward motion at least for low flight velocity. The screech enhancement by flight velocity in the higher  $M_j$  case has also been identified through screech effects on the model jet dynamics. In particular, shock oscillations and jet large scale whipping motion have been related to screech and their amplitude has been seen to be emphasized at higher  $M_j$ .

The screech frequency evolution in flight has been deduced from detailed near field acoustic signals. The prediction formula from Bryce and Pinker<sup>13</sup> has been investigated with particular expressions for the convection velocity, whereas the flight effect on shock cell length has been modeled following Morris.<sup>27</sup> For modes B and b, it has been shown that the convection velocity estimate as  $U_c = \alpha U_j$ , with  $\alpha$  being mode dependent, provides a very good frequency prediction. In particular, the slope of  $f_s$  with  $M_j$  has been adequately predicted. This result gives support to the case of Sarohia and Massier<sup>29</sup> that the boundary layer on the outer wall of the model jet nozzle shields the supersonic jet from the secondary flow. Some frequency jumps have been observed while the flight Mach number  $M_j$  has been increased. The screech mode evolution with  $M_j$  has been investigated from time signals and none of the frequency jumps could be related to a screech azimuthal mode change. It does not mean that screech was exactly identical on each side of a jump but only that the structure of the azimuthal instability mode related to screech remained unchanged across the observed discontinuities. Some work is still to be done to reveal the origin of the frequency jumps. It is believed that additional flow measurements, such as convective velocity measurements, should be able to further characterize and differentiate the screech modes arising from forward flight effects.

## ACKNOWLEDGMENTS

This research has been funded by the French Research Agency (Agence Nationale de la Recherche) through the ANR-10-BLAN-937-01 project JESSICA. The authors wish to express their most sincere thanks to Emmanuel Jondeau and Jean-Michel Perrin for their help in setting up the experiments.

- <sup>1</sup>A. Powell, "On the mechanism of choked jet noise," *Proc. Phys. Soc. London* **66**(408), 1039 (1953).
- <sup>2</sup>M. Merle, "Sur la fréquence des ondes émises par un jet d'air à grande vitesse," *Compte-Rendu de l'Académie des Sciences de Paris*, **243**, 490 (1956).
- <sup>3</sup>M. G. Davies and D. E. S. Oldfield, "Tones from a choked axisymmetric jet. I. Cell structure, eddy velocity and source locations," *Acustica* **12**(4), 257 (1962).
- <sup>4</sup>M. G. Davies and D. E. S. Oldfield, "Tones from a choked axisymmetric jet. II. The self excited loop and mode of oscillation," *Acustica* **12**(4), 267 (1962).
- <sup>5</sup>C. K. W. Tam, J. M. Seiner, and J. C. Yu, "Proposed relationship between broadband shock associated noise and screech tones," *J. Sound Vib.* **110**(2), 309 (1986).
- <sup>6</sup>A. Powell, Y. Umeda, and R. Ishii, "Observations of the oscillation modes of choked circular jets," *J. Acoust. Soc. Am.* **92**(5), 2823 (1992).
- <sup>7</sup>M. K. Ponton and J. M. Seiner, "Acoustic study of B helical mode for choked axisymmetric nozzle," *AIAA J.* **33**(3), 413 (1995).

- <sup>8</sup>G. Raman, "Advances in understanding supersonic jet screech: Review and perspective," *Prog. Aerosp. Sci.* **34**(1-2), 45 (1998).
- <sup>9</sup>G. Raman, "Supersonic jet screech: Half-century from Powell to the present," *J. Sound Vib.* **225**(3), 543 (1999).
- <sup>10</sup>J. A. Hay and E. G. Rose, "In-flight shock cell noise," *J. Sound Vib.* **11**(4), 411 (1970).
- <sup>11</sup>C. K. W. Tam, "Jet noise generated by large-scale coherent motion," *Aeroacoustics of Flight Vehicles: Theory and Practice*, Noise sources Vol. 1, edited by H. H. Hubbard (Nasa Reference Publication, Woodbury, NY, 1991), pp. 311–390.
- <sup>12</sup>A. Michalke and U. Michel, "Prediction of jet noise in flight from static tests," *J. Sound Vib.* **67**(3), 341 (1979).
- <sup>13</sup>W. D. Bryce and R. A. Pinker, "The noise from unheated supersonic jets in simulated flight," AIAA Paper No. 77-1327, 1977.
- <sup>14</sup>T. D. Norum and J. G. Shearin, "Effects of simulated flight on the structure and noise of underexpanded jets," NASA Technical Paper 2308, 1984.
- <sup>15</sup>A. Krothapalli, P. T. Soderman, C. S. Allen, J. A. Hayes, and S. M. Jaeger, "Flight effects on the far-field noise of a heated supersonic jet," *AIAA J.* **35**(6), 952 (1997).
- <sup>16</sup>T. D. Norum and J. G. Shearin, "Shock noise from supersonic jets in simulated flight to Mach 0.4," AIAA Paper No. 86-1945, 1986.
- <sup>17</sup>K. Viswanathan and M. J. Czech, "Measurement and modeling of effect of forward flight on jet noise," *AIAA J.* **49**(1), 216 (2011).
- <sup>18</sup>W. H. Brown, K. K. Ahuja, and C. K. W. Tam, "High speed flight effects on shock associated noise," AIAA Paper No. 86-1944, 1986.
- <sup>19</sup>T. D. Norum and M. C. Brown, "Simulated high speed flight effects on supersonic jet noise," AIAA Paper No. 93-4388, 1993.
- <sup>20</sup>J. D. Anderson, *Modern Compressible Flow with Historical Perspective*, 2nd ed. (McGraw-Hill, New York, 1990).
- <sup>21</sup>F. H. Champagne and I. J. Wignanski, "An experimental investigation of coaxial turbulent jets," *Int. J. Heat Mass Transfer* **14**(9), 1445 (1971).
- <sup>22</sup>J. M. Seiner and T. D. Norum, "Aerodynamic aspects of shock containing jet plumes," AIAA Paper No. 80-965, 1980.
- <sup>23</sup>K. Viswanathan, "Best practices for accurate measurement of pure jet noise," *Int. J. Aeroacoust.* **9**(1-2), 145 (2010).
- <sup>24</sup>K. C. Massey and K. K. Ahuja, "Screech frequency prediction in light of mode detection and convection speed measurements for heated jets," AIAA Paper No. 97-1625, 1997.
- <sup>25</sup>H. E. Plumblee, "Effects of forward velocity on turbulent jet mixing noise," NASA Contractor Report 2702, 1976.
- <sup>26</sup>J. Panda, G. Raman, and K. B. M. Q. Zaman, "Underexpanded screeching jets from circular, rectangular and elliptic nozzles," AIAA Paper No. 97-1623, 1997.
- <sup>27</sup>P. J. Morris, "A note on the effect of forward flight on shock spacing in circular jets," *J. Sound Vib.* **121**(1), 175 (1988).
- <sup>28</sup>T. D. Norum and J. G. Shearin, "Shock structure and noise of supersonic jets in simulated flight to Mach 0.4," NASA Technical Paper 2785, 1988.
- <sup>29</sup>V. Sarohia and P. F. Massier, "Effects of external boundary-layer flow on jet noise in flight," *AIAA J.* **15**(5), 659 (1977).
- <sup>30</sup>A. Michalke and G. Hermann, "On the inviscid instability of a circular jet with external flow," *J. Fluid Mech.* **114**, 343 (1982).
- <sup>31</sup>R. K. Amiet, "Correction of open jet wind tunnel measurements for shear layer refraction," AIAA Paper No. 75-532, 1975.
- <sup>32</sup>R. K. Amiet, "Refraction of sound by a shear layer," *J. Sound Vib.* **58**(4), 467 (1978).
- <sup>33</sup>K. K. Ahuja, H. K. Tanna, and B. J. Tester, "An experimental study of transmission, reflection and scattering of sound in a free jet flight simulation facility and comparison with theory," *J. Sound Vib.* **75**(1), 51 (1981).
- <sup>34</sup>R. H. Schlinker and R. K. Amiet, "Shear layer refraction and scattering of sound," AIAA Paper No. 80-973, 1980.
- <sup>35</sup>B. André, T. Castelain, and C. Bailly, "Shock-tracking procedure for studying screech-induced oscillations," *AIAA J.* **49**(7), 1563 (2011).
- <sup>36</sup>J. Panda, "Shock oscillation in underexpanded screeching jets," *J. Fluid Mech.* **363**, 173 (1998).
- <sup>37</sup>V. Sarohia, S. P. Parthasarathy, P. F. Massier, and G. Banerian, "Noise radiation from supersonic underexpanded jets in flight," AIAA Paper No. 80-1032, 1980.
- <sup>38</sup>V. Sarohia, "Some flight simulation experiments on jet noise from supersonic underexpanded flows," *AIAA J.* **16**(7), 710 (1978).